nanomaterials

MDPI

Article

Facile Synthesis of B/P Co-Doping Multicolor Emissive Carbon Dots Derived from Phenylenediamine Isomers and Their Application in Anticounterfeiting

Zhiwei Li [1,2]

[1] Key Laboratory for Polymeric Composite and Functional Materials of Ministry of Education, School of Chemistry, Sun Yat-sen University, Guangzhou 510275, China; lizhw36@mail2.sysu.edu.cn
[2] State Key Laboratory of Optoelectronic Materials and Technologies, Sun Yat-sen University, Guangzhou 510275, China

Abstract: Carbon dots (CDs) possess a considerable number of beneficial features for latent applications in biotargeted drugs, electronic transistors, and encrypted information. The synthesis of fluorescent carbon dots has become a trend in contemporary research, especially in the field of controllable multicolor fluorescent carbon dots. In this study, an elementary one-step hydrothermal method was employed to synthesize the multicolor fluorescent carbon dots by co-doping unique phenylenediamine isomers (o-PD, m-PD, and p-PD) with B and P elements, which under 365 nm UV light exhibited signs of lavender-color, grass-color, and tangerine-color fluorescence, respectively. Further investigations reveal the distinctness in the polymerization, surface-specific functional groups, and graphite N content of the multicolor CDs, which may be the chief factor regarding the different optical behaviors of the multicolor CDs. This new work offers a route for the exploration of multicolor CDs using B/P co-doping and suggests great potential in the field of optical materials, important information encryption, and commercial anticounterfeiting labels.

Keywords: phenylenediamine; isomer; multicolor CDs; co-doping; anticounterfeiting

Citation: Li, Z. Facile Synthesis of B/P Co-Doping Multicolor Emissive Carbon Dots Derived from Phenylenediamine Isomers and Their Application in Anticounterfeiting. *Nanomaterials* **2024**, *14*, 813. https://doi.org/10.3390/nano14100813

Academic Editor: Michael Tiemann

Received: 15 April 2024
Revised: 3 May 2024
Accepted: 4 May 2024
Published: 7 May 2024

1. Introduction

With the increasing progress and iterations of science and technology, research on carbon materials has attracted increasing attention in recent years. This includes investigations into various carbon-based materials such as graphene, carbon nanotubes, carbon nanofibers, fullerenes, and carbonaceous materials. Since 2000, carbon dots (CDs) materials have gained popularity owing to their exceptional luminescent properties [1–6]. In 2004, researchers such as Xu unexpectedly discovered unknown carbon-based fluorescent nanoparticles while separating single-walled carbon nanotubes using arc discharge soot, making the first instance of CD preparation [7]. From then on, researchers began to study this new type of material, especially in the field of luminescence [8–11]. In 2006, the Sun research team obtained nano-level carbonaceous grains through the laser ablation of carbon targets. After passivation, the prepared carbon particles exhibited significant fluorescence emission, which led to the novel concept of carbon dots being proposed in the scientific community to describe this unusual type of carbon particle [12]. As a general rule, CDs are spherical nanoparticles, typically zero-dimensional carbon nanomaterials with a dimension smaller than 10 nm, consisting of carbon nuclei and specific surface functional groups.

Until now, the various available types of carbon point synthesis can be generally grouped into two categories: top-down and bottom-up [13,14]. Due to the harsh conditions in the top-down preparation of CDs, complex subsequent processing steps are often required to obtain good samples, which is not suitable for large-scale production. Accordingly, the bottom-up synthesis of CDs has lower requirements for reaction equipment and relatively simple and feasible experimental conditions, meaning that it is gradually becoming

a commonly used method for preparing carbon dots. The methods for synthesizing CDs from bottom to top include the combustion method, hydrothermal method, thermal decomposition method, microwave-assisted method, and solvothermal method, among others. The traditional hydrothermal method is an economical, convenient, and environmentally friendly preparation method that has a wide range of easily obtainable precursor sources, such as natural products, biomaterials, and small molecule monomers. The carbon dots prepared using the hydrothermal method not only have a relatively simple postprocessing process but also have excellent optical properties. In 2012, researcher Yang and co-workers synthesized carbon dots using a simple one-step hydrothermal technique [15]. However, making the simple precursor using the hydrothermal method can easily lead to random products being obtained in high-temperature and high-pressure experimental reactions, making it difficult to control the specific chemical structure and physical and chemical properties of the obtained CDs. Recent studies have proposed heteroatom doping using elements such as N, S, B, and P to improve the fluorescence properties of CDs compared with those of the nondoped ones or those doped in different ways [16–23]. CDs doped with different heteroatoms will contribute to improving applications in the fields of encryption [24–29]. Therefore, we have found an original material for producing carbon dots, namely phenylenediamine. Phenylenediamine has three isomers (o-PD, m-PD, and p-PD), which can generate the sp2 domain and are beneficial for multicolor carbon dots [30–34]. The amino groups not only provide N-doped and hydrophilic functional groups but also offer a heteroatom binding site [14,35,36].

Here, in this detailed work, we explored a new approach to double heteroatoms co-doping for the synthetic route of multicolor CDs to achieve multicolor optical performance with an emission-tunable color. Using phenylenediamine isomers (o-PD, m-PD, and p-PD) as precursors, and commercial boric acid and commercial phosphoric acid as dopants in the coordination process, the specific CDs (L-CDs, G-CDs, and T-CDs) could be acquired using hydrothermal technology at a temperature of 180 °C for 12 h. As displayed in Scheme 1, resulting from B and P double heteroatoms doping, the as-prepared CDs of L-CDs, G-CDs, and T-CDs exhibited a lavender color, grass color, and tangerine color under irradiation with 365 nm ultraviolet rays, respectively. Furthermore, inspired by the tunable color phenomenon, we demonstrate that synthetic fluorescent ink containing CDs and CDs/PVA film, through the integration of CDs into the PVA matrix, can be used in anticounterfeiting applications, such as for transmitting encrypted information or anticounterfeiting labels.

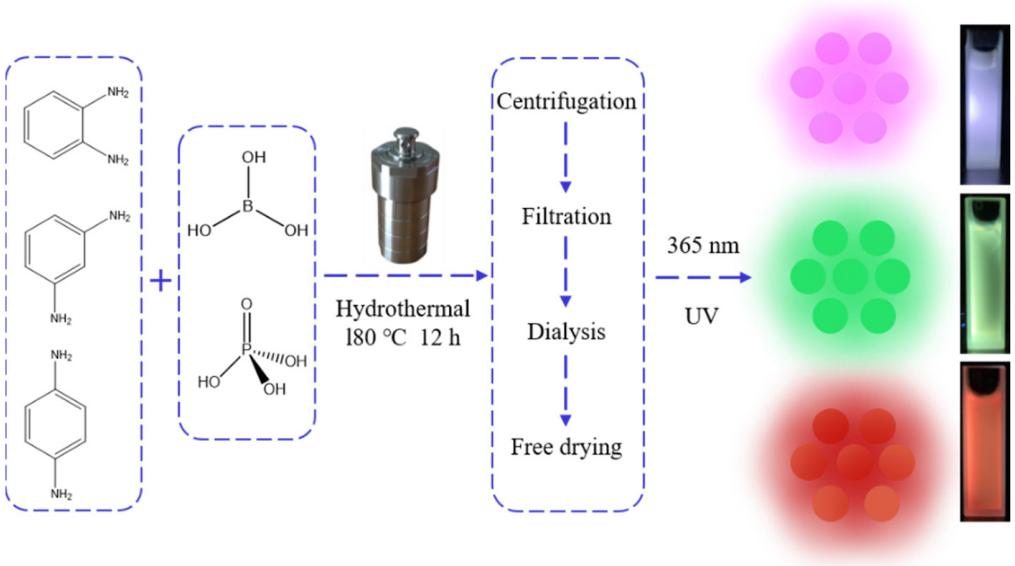

Scheme 1. Diagrammatic sketch of the synthetic process for obtaining multicolor CDs (L-CDs, G-CDs, and T-CDs).

2. Materials and Methods

2.1. Materials

o-phenylenediamine (o-PD), m-phenylenediamine (m-PD), p-phenylenediamine (p-PD), boric acid, phosphoric acid, and polyvinyl alcohol (PVA) were bought from Shanghai Macklin Biochemical Co., Ltd., (Shanghai, China). The dialysis membrane (cutoff, 1000 Da) was purchased from Viskase Union Carbide Corporation American Co., Ltd. (Bedford Park, IL, USA). All chemicals were used in this study as received without further purification. Deionized water was used throughout this study.

2.2. Synthesis of Multicolor CDs

In a straightforward process, 2 mL of phosphoric acid and 1.0 g of boric acid were dissolved in 23 mL of deionized water, producing a clear dispersion. A measure of 108.1 mg of o-PD was added into the above solution, which was stirred for 10 min. Then, the resultant precursor solution was transferred into a commercial 50 mL Teflon-lined autoclave, heated at 180 °C for 12 h, and subsequently naturally cooled down to room temperature. The obtained mixture was first collected using centrifugation, filtered with membrane filters with a pore size of 0.22 μm, and then dialyzed using a dialysis membrane (1000 Da) for 24 h. The powders were prepared from the dialyzed solution by freeze-drying. The resulting solids were redispersed in deionized water to obtain solutions of L-CDs. The synthetic procedure for G-CDs and T-CDs was similar to that for L-CDs, except that the precursor o-PD was replaced with m-PD or p-PD.

2.3. Preparation of the Encrypted Ink

An aqueous dispersion (50 mg/mL) of CDs can be used as encrypted ink for anticounterfeiting purposes.

2.4. CDs/PVA Film Preparation

To obtain the specific CDs/PVA nanocomposite, first, 1 g of PVA was completely dissolved in a 30 mL aqueous suspension of CDs. Then, the above solution underwent constant magnetic stirring for 2 h at 90 °C and was transferred to glass sheets, which were put into an oven at 100 °C for 3 h to evaporate the moisture content. The film was then cut into suitable shapes for future applications.

2.5. Characterization

Transmission electron microscopy (TEM) and high-resolution transmission electron microscopy (HR-TEM) images were obtained using a JEM-2100 transmission microscope (JOEL, Tokyo, Japan, 200 KV). The selected mode is low-dose and the exposure time is 0.5 s. X-ray diffraction (XRD) patterns were recorded using a PANalytical EMPYREAN III X'Pert spectrometer. The anode material of XRD is Cu and its radiate wavelength is 1.54 Å. Fourier transform infrared (FT-IR) spectra of the multicolor CDs were measured with a spectrometer (PerkinElmer Frontier, Waltham, MA, USA) with an attenuated total reflection (ATR) mode. X-ray photoelectron spectroscopy (XPS) spectra were obtained using a Thermo-VG Scientific ESCALAB 250 photoelectron spectrometer. The anode material is Al target and the wavelength is 8 Å. The UV–vis absorption spectra were recorded with a Cary 5000 UV–vis spectrophotometer (Agilent Technology (China) Co., Ltd., Beijing, China). The fluorescent spectrum, fluorescence lifetime, and absolute fluorescence quantum yield (FQY) data were investigated using an Edinburgh FLS1000 fluorescence spectrophotometer. The power used for the fluorescence measurements is 450 W. The color coordinates (CIE) were analyzed using Color Calculator software (CIE1931xy.V.1.6.0.2).

3. Results and Discussion

The multicolor carbon dots in this study were synthesized using a facile bottom-up approach, which is a simple, accessible, and fast method [37–40]. The required multicolored carbon dots were synthesized with co-doping phenylenediamine isomers (o-PD, m-PD, and

p-PD) using boric acid and phosphoric acid, and the prepared carbon dots were used as an encryption material. The specific situation details are outlined in the following subsection.

3.1. Structural Characterization of the Multicolor CDs

The appearance, microstructure, and particle dimensions of the multicolor CDs (L-CDs, G-CDs, and T-CDs) were verified using TEM. The morphology maps in Figure 1a–c clearly indicate that the prepared multicolor CDs are monodispersed nanoparticles without evident agglomeration. The HRTEM graphics in Figure 1d–f show that all three CDs have specific lattice fringes accompanied by ~0.21 nm lattice spacing, which is related to the graphitic carbon (100) diffraction plane, proving that the obtained CDs have a structure analogous to graphite [41]. As shown in Figure 1g–i, the dimension distributions of L-CDs, G-CDs, and T-CDs are normal distributions, with average particle sizes of 3.55 nm, 3.60 nm, and 3.70 nm, respectively. It is evident that the size of CD particles slowly increases along with the luminescence wavelength, which may cause a bathochromic shift in the luminescence wavelength of the multicolor CDs.

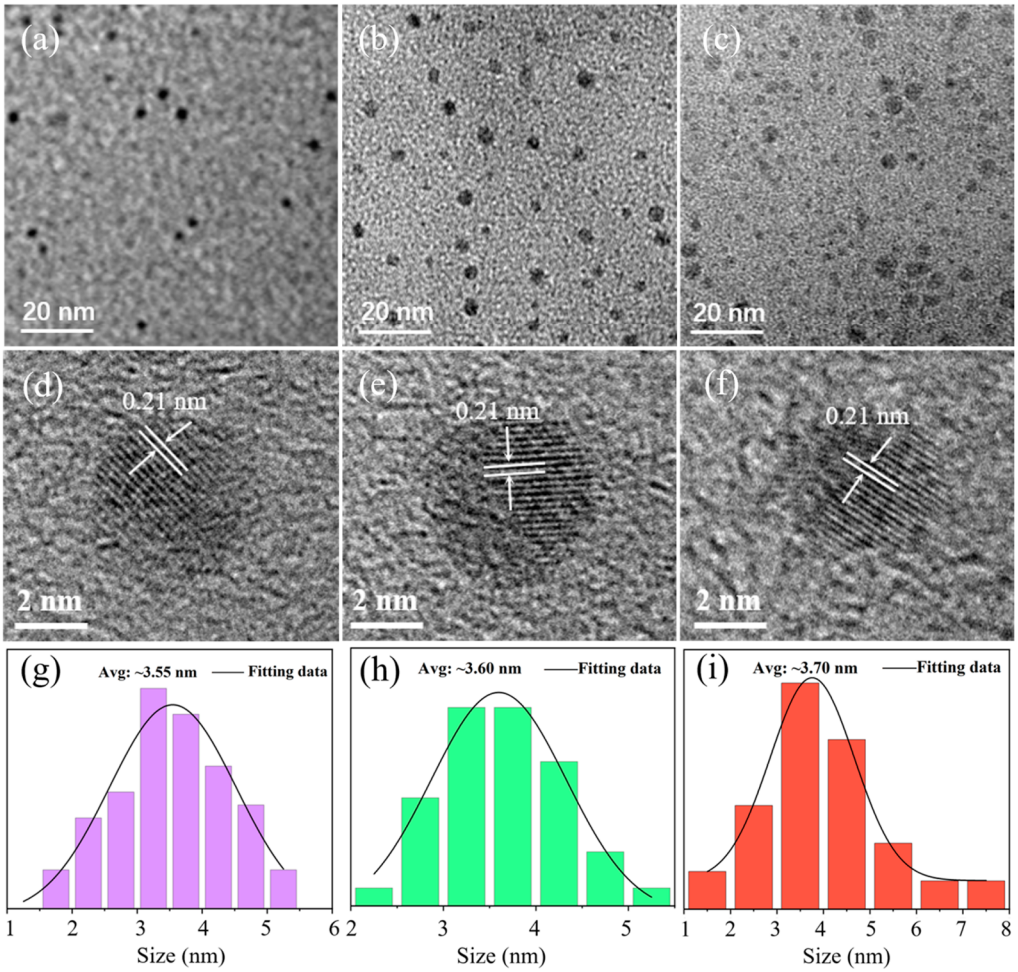

Figure 1. (**a**–**c**) TEM graphics of L-CDs, G-CDs, and T-CDs. (**d**–**f**) HRTEM graphics of L-CDs, G-CDs, and T-CDs. (**g**–**i**) The corresponding size distribution of L-CDs, G-CDs, and T-CDs.

The obtained XRD patterns of the specific CDs in Figure 2a show an expansive diffraction peak at approximately 27°, which indicates there are signs of carbonization present [32]. And the peak at this location indicates a random arrangement in the multicolor carbon dots powder structure. The multicolor CDs do not have distinct crystallinity, which may be explained by heteroatom (B or P) doping or sp3 C defects in the carbon structure [18,42,43]. Additionally, the chemical bonds and surface functional groups of CDs were measured by observing the FT-IR spectra shown in Figure 2b. The three CDs showed broad FTIR

absorptions from ~2500 to 3650 cm^{-1}, assigned to the stretching vibrations of O-H, N-H, and C-H [18,44]. The corresponding peaks at 1610, 1473, and 1403 cm^{-1} are attributed to C=C stretch vibration, N-H stretch vibration, and C-N stretch vibration, respectively [45]. Finally, the characteristic peaks at approximately 1186, 1011, and 864 cm^{-1} resulted from the stretch vibration of P=O, N–P, and B–O bonds, respectively [44,46].

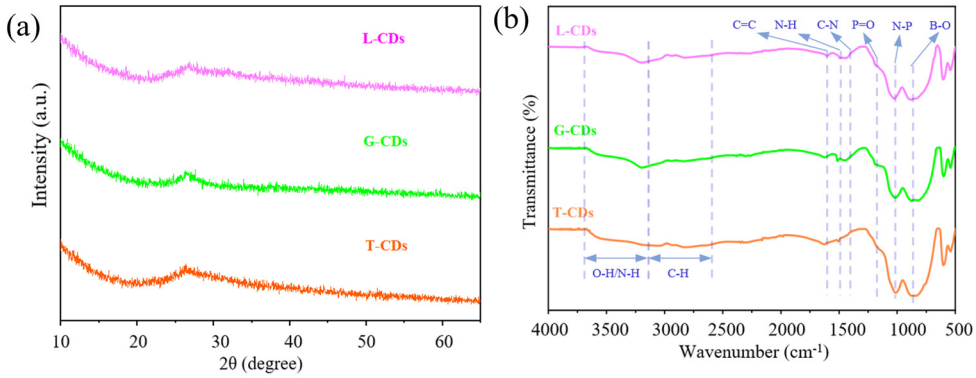

Figure 2. (**a**) XRD patterns of L-CDs, G-CDs, and T-CDs. (**b**) FTIR spectra of L-CDs, G-CDs, and T-CDs.

XPS was performed to further explore the functional groups and chemical composition of the multicolor CDs. As shown in Figure 3a–c, the whole XPS spectra of the L-CDs, G-CDs, and T-CDs indicated five characteristic peaks at approximately 533, 401, 285, 192, and 134 eV, for O 1s, N 1s, C 1s, B 1s, and P 2p, respectively. These peaks suggest that the three prepared CDs are composed of C, N, O, B, and P. The contents of C 1s, N 1s, O 1s, B 1s, and P 2p in the multicolor CDs are listed in Table 1. The data show increasing intensities of the C 1s, N 1s, and O 1s peaks with a redshift in PL emission. In Figure 3d–f, the C1s spectra of three dissimilar CDs are deconvoluted into four peaks at approximately 284.4 eV, 285.1 eV, 286.1 eV, and 288.5 eV, which correspond to C-C/C=C, C-N, -O-C=O, and C-O bonds, respectively [47–50]. The fitting XPS spectra of the N 1s of the multicolor CDs in Figure 3g–i indicate that the N 1s spectra may be mainly decomposed into four peaks at B–N (399.1 eV), pyridine N (400.7 eV), pyrrole N (401.7 eV), and graphitic N (402.4 eV) [51,52]. It is evident that the concentration of graphite N slowly increased in the high-resolution N 1s spectrum from L-CDs to T-CDs. It is also noticed that graphite N doping appeared to decrease the band gap and energy level of excited electrons transition, which could cause an obvious bathochromic shift [53]. The XPS O 1s spectra in multicolor CDs mainly contain three types of oxygen bonds that can be assigned to C=O (531.2 eV), C–O–C (532.5 eV), and C–O/P–O (533.8 eV), as shown, respectively, in Figure 3g–l [30]. Furthermore, in Figure S1a–c, deconvolution of the B 1s spectra of the multicolor CDs expresses B-N, B-O, and B-CO_2 bonds located at approximately 190.1 eV, 191.4 eV, and 192.8 eV, respectively [54]. The high-resolution P 2p spectra of the multicolor CDs could be deconvoluted into two peaks, exhibiting two peaks at 133.9 eV and 134.9 eV for P-O/P=O and P-N bonds, which are shown in Figure S1d–f [17].

Table 1. Contents (percent) of C, O, N, B, and P in the multicolor CDs.

Sample	C (%)	O (%)	N (%)	B (%)	P (%)
L-CDs	14.23	49.40	2.24	22.20	11.92
G-CDs	13.83	53.42	1.87	20.64	10.23
T-CDs	17.61	53.07	2.32	17.93	9.06

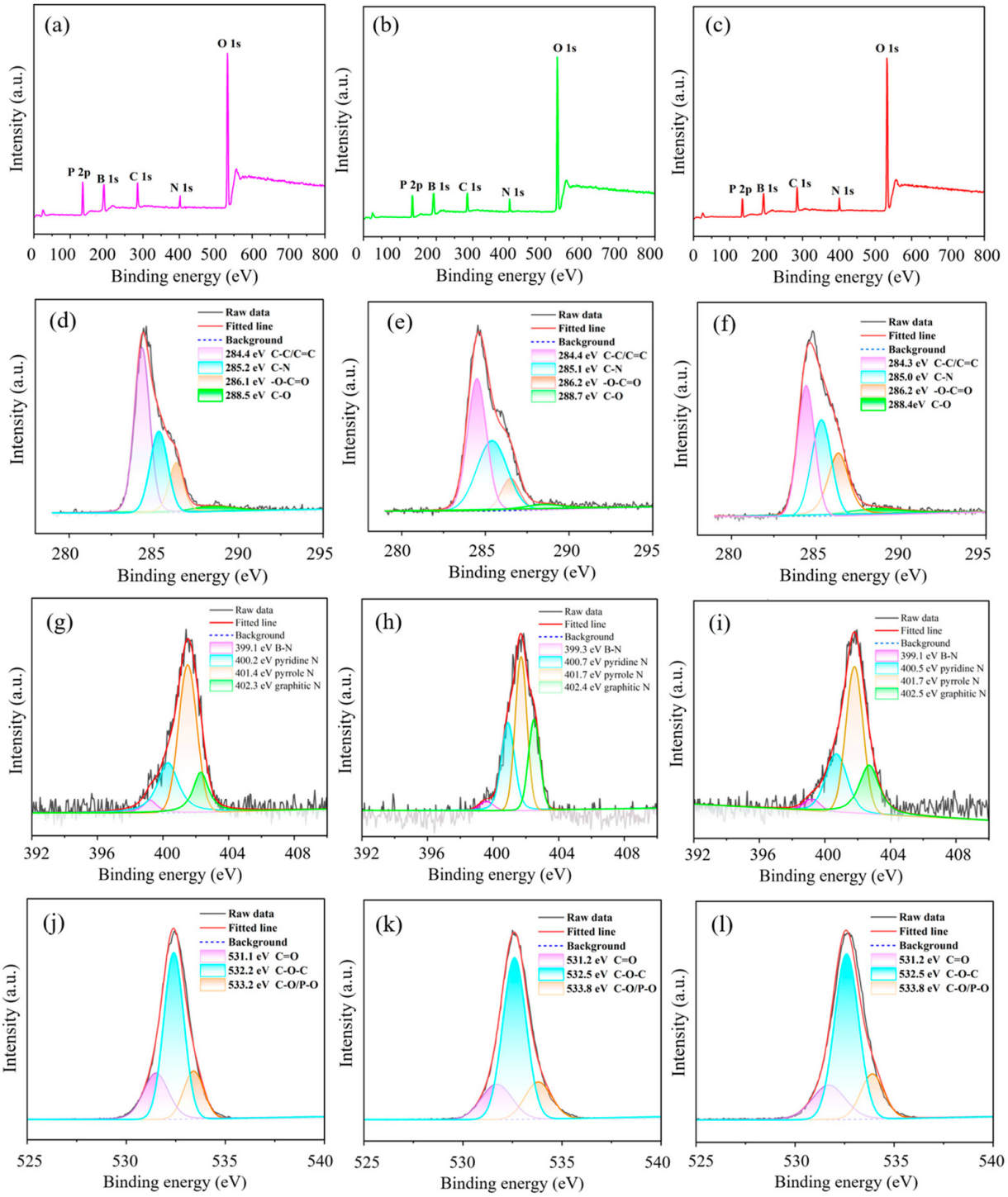

Figure 3. (**a**–**c**) XPS spectra of L-CDs, G-CDs, and T-CDs. (**d**–**f**) High-resolution XPS spectra of C 1s for L-CDs, G-CDs, and T-CDs. (**g**–**i**) High-resolution XPS spectra of N 1s for L-CDs, G-CDs, and T-CDs. (**j**–**l**) High-resolution XPS spectra of O 1s for L-CDs, G-CDs, and T-CDs.

3.2. Optical Performance of the Multicolor CDs

The UV–vis absorption and fluorescent spectra of the multicolor CDs (L-CDs, G-CDs, and T-CDs) in an aqueous solution were analyzed to explore their optical properties, which exhibit a noticeable multicolor tunable fluorescence emission. As shown in Figure 4a–c, the UV–vis absorption spectra of the multicolor CDs showed two clusters of UV absorption peaks, one set of peaks at 218, 230, and 235 nm; and another set at 274, 282, and 283 nm,

respectively. The stronger absorption peaks of the multicolor CDs are due to π–π* transitions of C=C and C=N bonds in the benzene ring microstructure [53]. And another weaker absorption peak corresponds to the n–π* transition of C=O/C=N [55]. Among L-CDs, G-CDs, and T-CDs, the absorption peak intensity in the ultraviolet area increased, clearly demonstrating that the content of N-containing aromatic rings increased. The diverse absorption bands of the multicolor CDs verified the different surface functional states of the three prepared typical CDs. Under 365 nm UV light, they appeared as lavender-color, grass-color, and tangerine-color fluorescence, respectively, as displayed in Figure 4a–c inset [56]. Figure 4a–c indicates that the definitive excitation wavelengths of the multicolor CDs occur primarily at 344, 458, and 537 nm, and the optimal emitted peaks are located at 414, 515, and 619 nm, respectively. The above information demonstrates that the multicolor CDs have an emission redshift. The fitting 3D mapping of the L-CDs PL excitation and emission wavelengths shown in Figure 4d denotes one excitation center from 300 nm to 400 nm, instigating the two lavender-color fluorescence emission sources (414 nm and 483 nm). Differently, the fitting 3D mapping of G-CDs PL excitation and emission wavelengths has two unclear excitation centers from 300 nm to 500 nm, corresponding to a central emission center (515 nm), as shown in Figure 4e. A 3D mapping of T-CDs is recorded in Figure 4f, which has an obvious excitation center (537 nm) and two unclear mountain peaks of emission centers (619 nm and 675 nm). This excitation–emission 3D mapping for the multicolor CDs is aligned with optimal excitation and emission wavelengths for the multicolor CDs [57]. Meanwhile, the fluorescent quantum yield (FQY) for multicolor CDs was calculated to be 5.2%, 6%, and 4.5%, respectively. The specific optical parameters of the multicolor CDs are shown in Table S1. Related to the molar absorption coefficients of published data of the other CDs, the data of the prepared multicolor CDs is smaller [58]. The reason is that the purity of the prepared sample has not reached 100%, and there are still some impurities inside. Subsequently, the CIE coordinates for the multicolor CDs are shown in Figure 4g–i, which better explains the connection between optical properties and fluorescence colors. The CIE coordinates were observed to be (0.21, 0.24), (0.24, 0.46), and (0.66, 0.34), respectively. The CIE coordinate maps have a signal of the lavender color, grass color, and tangerine color, consistent with the fluorescence color of CDs observed using a 365 nm UV lamp. Furthermore, Figure 4j–l demonstrates the time-resolved fluorescence decay curves of L-CDs, G-CDs, and T-CDs separately. Through a fitting operation, the mean fluorescent lifetimes of the multicolor CDs were 4.02, 6.54, and 2.85 ns, respectively, which aligned well with previous fluorescence quantum yield data. The different fluorescence lifetimes observed in the multicolor CDs suggest that they have distinct luminescence mechanisms, as indicated by fitting the decay curves using the tri-exponential function. The average lifetimes of the multicolor CDs were calculated using Equation (1):

$$\tau_{avg} = A_1 e^{(-t/\tau_1)} + A_2 e^{(-t/\tau_2)} + A_3 e^{(-t/\tau_3)} \quad (1)$$

From Equation (1), τ_1 is mainly attributed to electron transition in the carbon core. At the same time, τ_2 and τ_3 are attributed to electron transition in the surface state, which suggests multicolor CDs have surface defect states [50,59,60]. The specific data are listed in Table 2.

Table 2. The fitting statistics from the fluorescent decay curves of multicolor CDs.

Sample	τ_1 (ns)	A_1 (%)	τ_2 (ns)	A_2 (%)	τ_3 (ns)	A_3 (%)
L-CDs	1.276	51.91	3.570	25.15	10.746	22.94
G-CDs	1.393	9.24	4.836	64.72	12.611	26.04
T-CDs	0.537	63.59	2.584	29.98	26.989	6.43

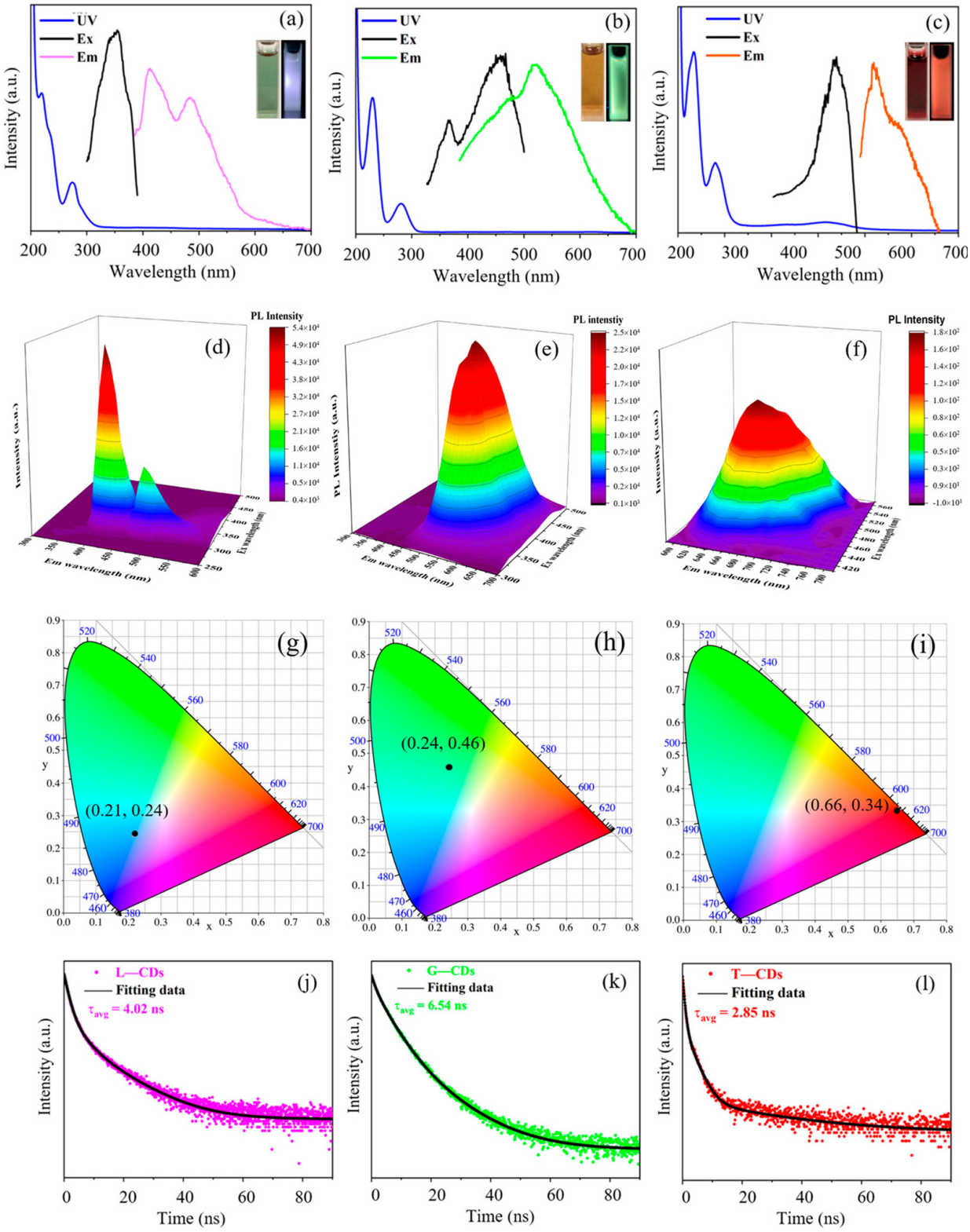

Figure 4. (**a**–**c**) UV–vis spectra, fluorescent excitation spectra, and emission spectra of the multicolor CDs (the scale is linear). The insets display the optical graphics of the multicolor CD solution in daylight (**left**) and a 365 nm UV light (**right**). (**d**–**f**) Three-dimensional fluorescent excitation–emission mapping for the multicolor CDs. (**g**–**i**) CIE coordinates of the multicolor CDs. (**j**–**l**) Time-resolved fluorescence decay curve of the multicolor CDs (the scale is logarithmic).

3.3. Multiemission Fluorescent Mechanism of the Multicolor CDs

On account of the acquired morphology and specific optical characterization results, the fluorescent mechanism of the multicolor CDs with alterable PL performance can be put forward. As shown in Figure 5, the multiemission distinguishing features of CDs depend on the synergistic action of the carbon core and surface functional defect state. In this study, heteroatom doping (B and P) was found to be conducive, producing more defective states of energy levels, which enables the capture of photoexcited electrons [61,62]. At the same time, the lattice doping of the heteroatom (B and P) increases the energy level between carbon π and carbon π^*, facilitating multiple routes of electron transferring (n $\rightarrow$ π^*) in PL emission. The different doping atom energy levels cause three radiated recombination steps to return to the ground state. Additionally, the synergistic action induced the emission of broader wavelengths via interband crossing, resulting in a redshifted wavelength of PL emission, which is shown as lavender color (414 nm), grass color (515 nm), and tangerine color (619 nm) [53,63–65]. Moreover, the rising carbonization degree and surface defects of the CDs play an important critical role in the area of PL emission.

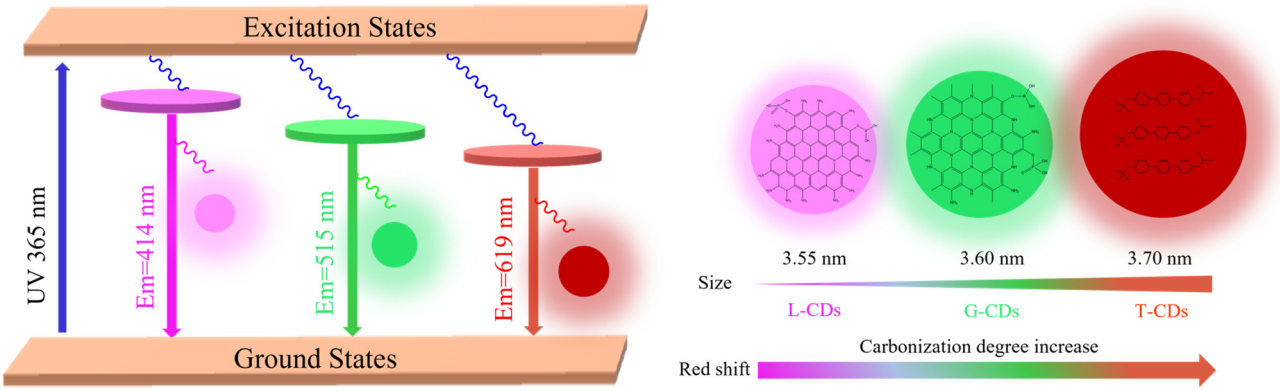

Figure 5. Proposed fluorescent mechanism of the multiemission CDs.

3.4. The Multicolor CDs for Encrypted Information and Anticounterfeiting Labels

Given that the prepared CDs (L-CDs, G-CDs, and T-CDs) display excellent optical performance and changeable multicolor fluorescent behavior, these materials have potential applications in the domain of message encryption and anticounterfeiting labels. Figure 6 reveals the information encryption utilization of the obtained three colored CDs (L-CDs, G-CDs, and T-CDs). The three patterns of Sun Yat-sen University were printed on nonfluorescent paper using multicolor CD inks containing L-CDs, G-CDs, and T-CDs, respectively. Furthermore, with the 365 nm UV light turning on, Figure 6a,b clearly indicates that three tunable pattern colors are visible. Once the UV lamp radiation is turned off, these printed patterns cannot be easily identified with the human eye in sunlight. These results are further proof that the fluorescent quantum yield (FQY) of the G-CDs is the best one among the synthesized CDs. In addition, multicolor CDs have been used to fabricate CDs/PVP films. As shown in Figure 6c, corresponding to the colors of the synthesized water-soluble CDs, the three CDs/PVA films also emit different colors under a UV lamp with 365 nm excitation, representing that the CDs/PVA film can be worked as a unique anticounterfeiting label [57]. These optical phenomena of multicolor CDs hold great promise for applications in the field of information encryption and transmission.

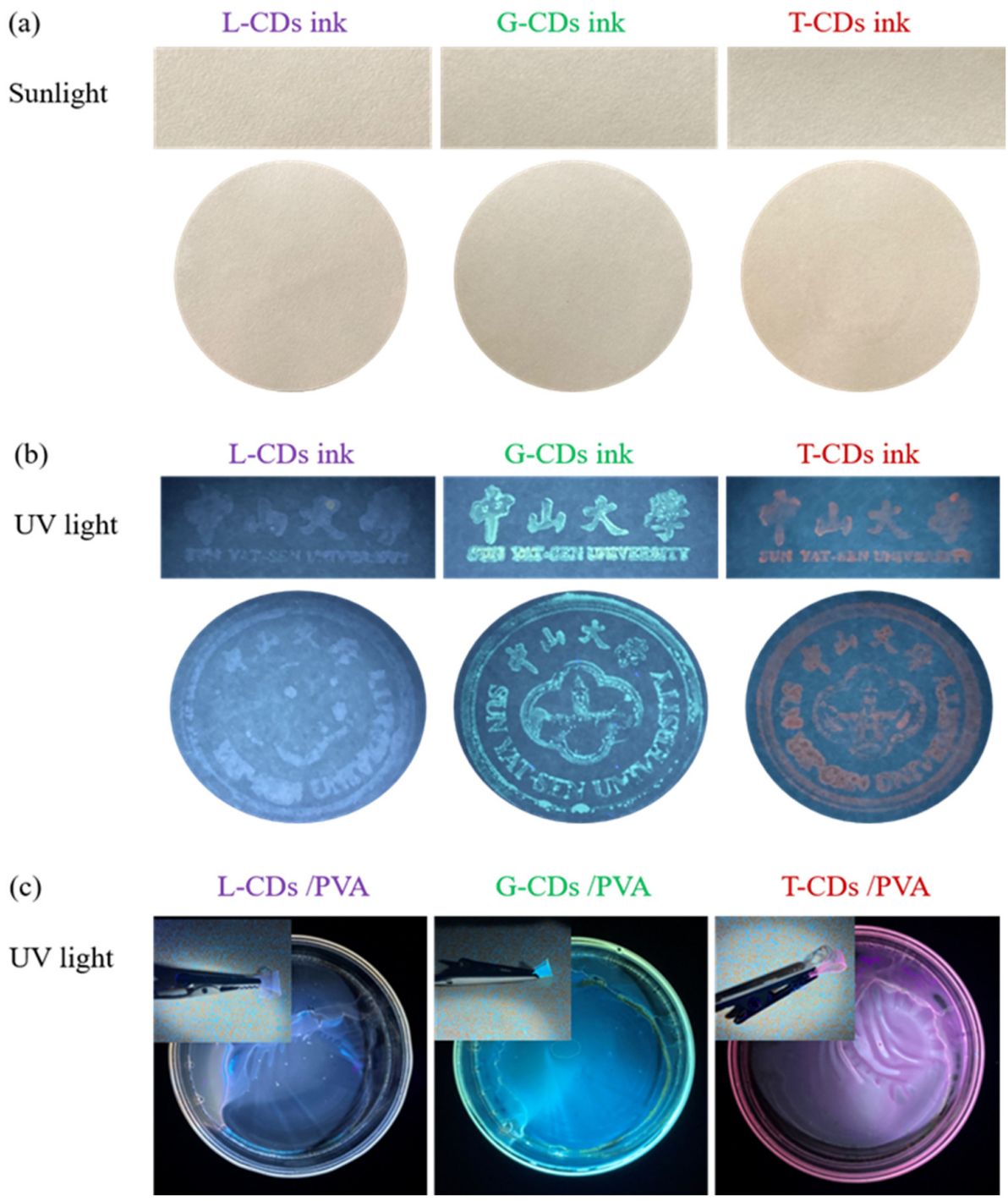

Figure 6. The anticounterfeiting graphics of the multicolor CDs (L-CDs, G-CDs, and T-CDs). The filter paper printed with Sun Yat-sen University patterns (**a**) with a daylight lamp and (**b**) in 365 nm UV light, respectively. (**c**) Photographs of fluorescent CDs/PVA films with different CDs in a petri dish with 365 nm UV light irradiation (inset: the flaky cutting film of the multicolor CDs/PVA).

4. Conclusions

In conclusion, by using phenylenediamine isomers as precursors and adding boric acid and phosphoric acid as doping reagents, we acquired lavender-color (414 nm), grass-color (515 nm), and tangerine-color (619 nm) fluorescence with a simple hydrothermal method. Surprisingly, the skip distance of emission has a large range from purple color to red color. In view of the measurement results, the optical performance of multicolor

CDs is ascribed to the cooperative effect of the core state and the surface functional group defect state of B and P doping. The reasonably regulatable fluorescence color of CDs has great commercialization potential in the areas of information encryption and commercial anticounterfeiting labels.

Supplementary Materials: The following supporting information can be downloaded at https://www.mdpi.com/article/10.3390/nano14100813/s1, Figure S1: (a–c) High-resolution XPS spectra of B 1s of L-CDs, G-CDs, and T-CDs. (d–f) High-resolution XPS spectra of P 2p of L-CDs, G-CDs, and T-CDs; Table S1: Specific optical parameters of the multicolor CDs.

Funding: This research received no external funding.

Data Availability Statement: The data presented in this study are available on request from the corresponding author.

Conflicts of Interest: The authors declare no conflicts of interest.

References

1. Yan, Y.; Gong, J.; Chen, J.; Zeng, Z.; Huang, W.; Pu, K.; Liu, J.; Chen, P. Recent Advances on Graphene Quantum Dots: From Chemistry and Physics to Applications. *Adv. Mater.* **2019**, *31*, e1808283. [CrossRef]
2. Xia, C.L.; Zhu, S.J.; Feng, T.L.; Yang, M.X.; Yang, B. Evolution and Synthesis of Carbon Dots: From Carbon Dots to Carbonized Polymer Dots. *Adv. Sci.* **2019**, *6*, 1901316. [CrossRef]
3. Baker, S.N.; Baker, G.A. Luminescent Carbon Nanodots: Emergent Nanolights. *Angew. Chem. Int. Ed.* **2010**, *49*, 6726–6744. [CrossRef]
4. Ragazzon, G.; Cadranel, A.; Ushakova, E.V.; Wang, Y.C.; Guldi, D.M.; Rogach, A.L.; Kotov, N.A.; Prato, M. Optical processes in carbon nanocolloids. *Chem* **2021**, *7*, 606–628. [CrossRef]
5. Wang, B.Y.; Lu, S.Y. The light of carbon dots: From mechanism to applications. *Matter* **2022**, *5*, 110–149. [CrossRef]
6. Ai, L.; Song, Z.Q.; Nie, M.J.; Yu, J.K.; Liu, F.K.; Song, H.Q.; Zhang, B.; Waterhouse, G.I.N.; Lu, S.Y. Solid-state Fluorescence from Carbon Dots Widely Tunable from Blue to Deep Red through Surface Ligand Modulation. *Angew. Chem. Int. Ed.* **2023**, *62*, e202217822. [CrossRef]
7. Xu, X.Y.; Ray, R.; Gu, Y.L.; Ploehn, H.J.; Gearheart, L.; Raker, K.; Scrivens, W.A. Electrophoretic analysis and purification of fluorescent single-walled carbon nanotube fragments. *J. Am. Chem. Soc.* **2004**, *126*, 12736–12737. [CrossRef]
8. Muthamma, K.; Sunil, D.; Shetty, P. Carbon dots as emerging luminophores in security inks for anti-counterfeit applications—An up-to-date review. *Appl. Mater. Today* **2021**, *23*, 101050. [CrossRef]
9. Li, J.R.; Gong, X. The Emerging Development of Multicolor Carbon Dots. *Small* **2022**, *18*, e2205099. [CrossRef]
10. Xu, A.L.; Wang, G.; Li, Y.Q.; Dong, H.; Yang, S.W.; He, P.; Ding, G.Q. Carbon-Based Quantum Dots with Solid-State Photoluminescent: Mechanism, Implementation, and Application. *Small* **2020**, *16*, e2004621. [CrossRef]
11. Wang, H.L.; Ai, L.; Song, H.Q.; Song, Z.Q.; Yong, X.; Qu, S.N.; Lu, S.Y. Innovations in the Solid-State Fluorescence of Carbon Dots: Strategies, Optical Manipulations, and Applications. *Adv. Funct. Mater.* **2023**, *33*, 2303756. [CrossRef]
12. Sun, Y.P.; Zhou, B.; Lin, Y.; Wang, W.; Fernando, K.A.S.; Pathak, P.; Meziani, M.J.; Harruff, B.A.; Wang, X.; Wang, H.F.; et al. Quantum-sized carbon dots for bright and colorful photoluminescence. *J. Am. Chem. Soc.* **2006**, *128*, 7756–7757. [CrossRef]
13. Qu, D.; Sun, Z.C. The formation mechanism and fluorophores of carbon dots synthesized via a bottom-up route. *Mater. Chem. Front.* **2020**, *4*, 400–420. [CrossRef]
14. Xue, S.S.; Li, P.F.; Sun, L.; An, L.; Qu, D.; Wang, X.Y.; Sun, Z.C. The Formation Process and Mechanism of Carbon Dots Prepared from Aromatic Compounds as Precursors: A Review. *Small* **2023**, *19*, e2206180. [CrossRef]
15. Zhu, S.J.; Zhang, J.H.; Wang, L.; Song, Y.B.; Zhang, G.Y.; Wang, H.Y.; Yang, B. A general route to make non-conjugated linear polymers luminescent. *Chem. Commun.* **2012**, *48*, 10889–10891. [CrossRef]
16. Yang, P.; Zhu, Z.Q.; Zhang, T.; Chen, M.Z.; Cao, Y.Z.; Zhang, W.; Wang, X.; Zhou, X.Y.; Chen, W.M. Facile synthesis and photoluminescence mechanism of green emitting xylose-derived carbon dots for anti-counterfeit printing. *Carbon* **2019**, *146*, 636–649. [CrossRef]
17. Zheng, Y.; Wang, Z.H.; Liu, J.W.; Zhang, Y.F.; Gao, L.; Wang, C.; Zheng, X.; Zhou, Q.; Yang, Y.; Li, Y.B.; et al. Long-Lived Room Temperature Phosphorescence Crystals with Green Light Excitation. *ACS Appl. Mater. Interfaces* **2022**, *14*, 15706–15715. [CrossRef]
18. Shen, J.; Xu, B.; Wang, Z.F.; Zhang, J.; Zhang, W.G.; Gao, Z.H.; Wang, X.; Zhu, C.F.; Meng, X.G. Aggregation-induced room temperature phosphorescent carbonized polymer dots with wide-range tunable lifetimes for optical multiplexing. *J. Mater. Chem. C* **2021**, *9*, 6781–6788. [CrossRef]
19. Wang, Z.F.; Shen, J.; Xu, B.; Jiang, Q.L.; Ming, S.L.; Yan, L.T.; Gao, Z.H.; Wang, X.; Zhu, C.F.; Meng, X.G. Thermally Driven Amorphous-Crystalline Phase Transition of Carbonized Polymer Dots for Multicolor Room-Temperature Phosphorescence. *Adv. Opt. Mater.* **2021**, *9*, 2100421. [CrossRef]

20. Song, X.; Sun, H.Y.; Yang, S.W.; Zhao, S.Z.; Liao, F. Synthesis of photoluminescent o-phenylenediamine-m-phenylenediamine copolymer nanospheres: An effective fluorescent sensing platform for selective and sensitive detection of chromium(VI) ion. *J. Lumin.* **2016**, *169*, 186–190. [CrossRef]
21. Barhum, H.; Alon, T.; Attrash, M.; Machnev, A.; Shishkin, I.; Ginzburg, P. Multicolor Phenylenediamine Carbon Dots for Metal-Ion Detection with Picomolar Sensitivity. *ACS Appl. Nano Mater.* **2021**, *4*, 9919–9931. [CrossRef]
22. Gong, X.; Li, W.J.; Wu, Y.Z.; Li, X.Y.; Ma, Y.; Wang, H.X.; Wu, M. A rational strategy for directly synthesizing strongly yellow solid-state fluorescent-emitting carbon nanodots composite microparticles by structure regulation. *Mater. Today Adv.* **2023**, *20*, 100428. [CrossRef]
23. Mao, X.; Zhao, X.; Hu, H.; Li, Z.Q.; Xiong, W.; Wei, Y.J.; Gao, W. One-step hydrothermal method synthesized pH-dependent carbon dots for multistage anti-counterfeiting. *Spectrochim. Acta Part A Mol. Biomol. Spectrosc.* **2023**, *303*, 123257. [CrossRef]
24. Qin, Y.; He, Y.; Song, G.W. Ultralong Room-Temperature Phosphorescence of Boron Carbon Oxynitride Nanodots Encapsulated in Pyrophosphate in Dry and Wet States for Fingerprint Detection and Information Protection. *ACS Appl. Nano Mater.* **2023**, *6*, 1360–1368. [CrossRef]
25. Wu, Y.Y.; Liu, L.; Zou, J.H.; Liu, J.Q.; Hu, Y.C.; Ban, C.Y.; Li, F.Y.; Li, Z.F.; Zhang, H.S.; Zhou, Z.; et al. Confining Carboxylized Carbon Nanotube for Phosphorescence Afterglow with Optical Memory Plasticity. *Adv. Opt. Mater.* **2022**, *10*, 2102323. [CrossRef]
26. Yang, L.; Zhang, Q.; Huang, Y.Y.; Luo, C.X.; Quan, Z.Y.; Li, H.J.; Sun, S.G.; Xu, Y.Q. A sequential dual-lock strategy for generation of room-temperature phosphorescence of boron doped carbon dots for dynamic anti-counterfeiting. *J. Colloid Interface Sci.* **2023**, *632*, 129–139. [CrossRef]
27. Liu, X.J.; Liu, W.F.; Zuo, K.; Zheng, J.X.; Wang, M.L.; Liu, X.G. High Color Stability Blue-to-Violet Room Temperature Phosphorescent Carbon Dot Composites with Ultralong Lifetime for Information Encryption. *ACS Sustain. Chem. Eng.* **2023**, *11*, 1809–1819. [CrossRef]
28. Jie, Y.N.; Wang, D.; Chen, R.F.; Zhang, J.Y.; Li, W.Q.; Huang, J.F.; Dai, P.G.; Gao, Y.; Li, F.C.; Fang, J.W. Deep-blue thermally activated delayed fluorescence carbon dots with ultralong lifetime. *Nanoscale* **2023**, *15*, 3337–3344. [CrossRef]
29. Sun, Y.J.; Lou, D.Y.; Liu, W.; Zheng, Z.K.; Chen, X.D. SERS Labels for Optical Anticounterfeiting: Structure, Fabrication, and Performance. *Adv. Opt. Mater.* **2023**, *11*, 2201549. [CrossRef]
30. Yan, F.; Li, J.R.; Zhao, X.J.; Gong, X. Unveiling Unconventional Luminescence Behavior of Multicolor Carbon Dots Derived from Phenylenediamine. *J. Phys. Chem. Lett.* **2023**, *14*, 5975–5984. [CrossRef]
31. Zhang, H.M.; Sun, L.L.; Guo, X.J.; Xu, J.Y.; Zhao, X.H.; Xia, Y.Z. Multicolor fluorescent/room temperature phosphorescent carbon dot composites for information encryption and anti-counterfeiting. *Appl. Surf. Sci.* **2023**, *613*, 155945. [CrossRef]
32. Jia, J.; Lu, W.; Cui, S.; Dong, C.; Shuang, S. Synthesis of multicolor luminescent adjustable carbon dots and their application in anti-counterfeiting. *Mater. Today Chem.* **2022**, *25*, 100972. [CrossRef]
33. Zheng, Y.; Zhou, Q.; Yang, Y.; Chen, X.H.; Wang, C.; Zheng, X.; Gao, L.; Yang, C.L. Full-Color Long-Lived Room Temperature Phosphorescence in Aqueous Environment. *Small* **2022**, *18*, e2201223. [CrossRef]
34. Xu, X.K.; Mo, L.Q.; Li, W.; Li, Y.D.; Lei, B.F.; Zhang, X.J.; Zhuang, J.L.; Hu, C.F.; Liu, Y.L. Red, green and blue aggregation-induced emissive carbon dots. *Chin. Chem. Lett.* **2021**, *32*, 3927–3930. [CrossRef]
35. Miao, S.H.; Liang, K.; Zhu, J.J.; Yang, B.; Zhao, D.Y.; Kong, B. Hetero-atom-doped carbon dots: Doping strategies, properties and applications. *Nano Today* **2020**, *33*, 100879. [CrossRef]
36. Wei, Z.T.; Lu, W.Y.; Wang, X.M.; Ni, J.P.; Prova, U.H.; Wang, C.X.; Huang, G.Y. Harnessing versatile dynamic carbon precursors for multi-color emissive carbon dots. *J. Mater. Chem. C* **2022**, *10*, 1932–1967. [CrossRef]
37. Tian, X.T.; Yin, X.B. Carbon Dots, Unconventional Preparation Strategies, and Applications Beyond Photoluminescence. *Small* **2019**, *15*, e1901803. [CrossRef]
38. Simoes, R.; Rodrigues, J.; Neto, V.; Monteiro, T.; Gonçalves, G. Carbon Dots: A Bright Future as Anticounterfeiting Encoding Agents. *Small* **2024**, *19*, e2311526. [CrossRef]
39. Yang, L.J.; An, Y.B.; Xu, D.Z.; Dai, F.; Shao, S.L.; Lu, Z.X.; Liu, G. Comprehensive Overview of Controlled Fabrication of Multifunctional Fluorescent Carbon Quantum Dots and Exploring Applications. *Small* **2024**, *28*, e2309293. [CrossRef] [PubMed]
40. Zhang, Y.Q.; Chen, L.; Liu, B.; Yu, S.P.; Yang, Y.Z.; Liu, X.G. Multicolor Afterglow Carbon Dots: Luminescence Regulation, Preparation, and Application. *Adv. Funct. Mater.* **2024**, *30*, 2315366. [CrossRef]
41. Yan, F.Y.; Jiang, Y.X.; Sun, X.D.; Wei, J.F.; Chen, L.; Zhang, Y.Y. Multicolor carbon dots with concentration-tunable fluorescence and solvent-affected aggregation states for white light-emitting diodes. *Nano Res.* **2020**, *13*, 52–60. [CrossRef]
42. Wan, Z.J.; Li, Y.M.; Zhou, Y.Z.; Peng, D.P.; Zhang, X.J.; Zhuang, J.L.; Lei, B.F.; Liu, Y.L.; Hu, C.F. High-Efficiency Solid-State Luminescence from Hydrophilic Carbon Dots with Aggregation-Induced Emission Characteristics. *Adv. Funct. Mater.* **2023**, *33*, 2207296. [CrossRef]
43. Xu, X.K.; Mo, L.Q.; Li, Y.D.; Pan, X.Q.; Hu, G.Q.; Lei, B.F.; Zhang, X.J.; Zheng, M.T.; Zhuang, J.L.; Liu, Y.L.; et al. Construction of Carbon Dots with Color-Tunable Aggregation-Induced Emission by Nitrogen-Induced Intramolecular Charge Transfer. *Adv. Mater.* **2021**, *33*, 2104872. [CrossRef]
44. Jiang, K.; Wang, Y.H.; Cai, C.Z.; Lin, H.W. Conversion of Carbon Dots from Fluorescence to Ultralong Room-Temperature Phosphorescence by Heating for Security Applications. *Adv. Mater.* **2018**, *30*, e1800783. [CrossRef]
45. Yuan, F.L.; Wang, Z.B.; Li, X.H.; Li, Y.C.; Tan, Z.A.; Fan, L.Z.; Yang, S.H. Bright Multicolor Bandgap Fluorescent Carbon Quantum Dots for Electroluminescent Light-Emitting Diodes. *Adv. Mater.* **2017**, *29*, 1604436. [CrossRef]

46. Li, W.; Zhou, W.; Zhou, Z.S.; Zhang, H.R.; Zhang, X.J.; Zhuang, J.L.; Liu, Y.L.; Lei, B.F.; Hu, C.F. A Universal Strategy for Activating the Multicolor Room-Temperature Afterglow of Carbon Dots in a Boric Acid Matrix. *Angew. Chem. Int. Ed.* **2019**, *58*, 7278–7283. [CrossRef]
47. Sohal, N.; Maity, B.; Basu, S. Morphology Effect of One-Dimensional MnO_2 Nanostructures on Heteroatom-Doped Carbon Dot-Based Biosensors for Selective Detection of Glutathione. *ACS Appl. Bio Mater.* **2022**, *5*, 2355–2364. [CrossRef]
48. Deng, Z.Q.; Liu, C.; Jin, Y.Z.; Pu, J.L.; Wang, B.; Chen, J.C. High quantum yield blue- and orange-emitting carbon dots: One-step microwave synthesis and applications as fluorescent films and in fingerprint and cellular imaging. *Analyst* **2019**, *144*, 4569–4574. [CrossRef]
49. Dai, R.Y.; Chen, X.P.; Ouyang, N.; Hu, Y.P. A pH-controlled synthetic route to violet, green, and orange fluorescent carbon dots for multicolor light-emitting diodes. *Chem. Eng. J.* **2022**, *431*, 134172. [CrossRef]
50. Zhang, H.M.; Guo, X.J.; Jian, K.; Fu, L.M.; Zhao, X.H. Rapid Preparation of Long-Wavelength Emissive Carbon Dots for Information Encryption Using the Microwave-Assisted Method. *Inorg. Chem.* **2023**, *62*, 13847–13856. [CrossRef]
51. Han, B.Y.; Lei, X.S.; Li, D.; Liu, Q.D.; Chen, Y.J.; Wang, J.; He, G.H. Shallow Traps in Carbon Nitride Quantum Dots to Achieve 6.47 s Ultralong Lifetime and Wavelength-Tunable Room Temperature Phosphorescence. *Adv. Opt. Mater.* **2023**, *11*, 2202293. [CrossRef]
52. Su, Q.; Yang, X.M. Promoting Room Temperature Phosphorescence through Electron Transfer from Carbon Dots to Promethazine. *ACS Appl. Mater. Interfaces* **2021**, *13*, 41238–41248. [CrossRef]
53. Holá, K.; Sudolská, M.; Kalytchuk, S.; Nachtigallová, D.; Rogach, A.L.; Otyepka, M.; Zboril, R. Graphitic Nitrogen Triggers Red Fluorescence in Carbon Dots. *ACS Nano* **2017**, *11*, 12402–12410. [CrossRef]
54. Wang, X.L.; Wang, S.Q.; Huang, Y.S.; Huang, L.M.; Sun, J.P.; Lin, Z.H. Full-color Persistent Room-temperature Phosphorescence from Carbon Dot Composites Based on a Single Nonaromatic Carbon Source. *Chem.-Asian J.* **2023**, *18*, e202201027. [CrossRef]
55. Lyu, B.W.; Li, H.J.; Xue, F.F.; Sai, L.M.; Gui, B.J.; Qian, D.J.; Wang, X.Y.; Yang, J.H. Facile, gram-scale and eco-friendly synthesis of multi-color graphene quantum dots by thermal-driven advanced oxidation process. *Chem. Eng. J.* **2020**, *388*, 124285. [CrossRef]
56. Gao, D.; Zhang, Y.S.; Liu, A.M.; Zhu, Y.D.; Chen, S.P.; Wei, D.; Sun, J.; Guo, Z.Z.; Fan, H.S. Photoluminescence-tunable carbon dots from synergy effect of sulfur doping and water engineering. *Chem. Eng. J.* **2020**, *388*, 124199. [CrossRef]
57. Guo, G.Q.; Li, T.T.; Wang, Y.R.; Hu, H.W.; Xing, H.M.; Tang, S.Y.; Gao, S.E.; Leng, X.; Chen, D. Aggregation-induced bimodal excitation of nitrogen-doped carbon dots for ratiometric sensing of new coccine and solid-state multicolor lighting. *J. Colloid Interface Sci.* **2023**, *645*, 96–106. [CrossRef]
58. Liang, W.X.; Ge, L.; Hou, X.F.; Ren, X.Y.; Yang, L.J.; Bunker, C.E.; Overton, C.M.; Wang, P.; Sun, Y.P. Evaluation of Commercial "Carbon Quantum Dots" Sample on Origins of Red Absorption and Emission Features. *C–J. Carbon Res.* **2019**, *5*, 70. [CrossRef]
59. Ding, Y.F.; Zheng, J.X.; Wang, J.L.; Yang, Y.Z.; Liu, X.G. Direct blending of multicolor carbon quantum dots into fluorescent films for white light emitting diodes with an adjustable correlated color temperature. *J. Mater. Chem. C* **2019**, *7*, 1502–1509. [CrossRef]
60. Wang, R.N.; Huang, Z.H.; Ding, L.F.; Yang, F.Y.; Peng, D. Carbon Dot Powders with Cross-Linking-Based Long-Wavelength Emission for Multicolor Imaging of Latent Fingerprints. *ACS Appl. Nano Mater.* **2022**, *8*, 2214–2221. [CrossRef]
61. Wang, J.L.; Li, Q.; Zheng, J.X.; Yang, Y.Z.; Liu, X.G.; Xu, B.S. N, B-Codoping Induces High-Efficiency Solid-State Fluorescence and Dual Emission of Yellow/Orange Carbon Dots. *ACS Sustain. Chem. Eng.* **2021**, *9*, 2224–2236. [CrossRef]
62. Macairan, J.R.; de Medeiros, T.V.; Gazzetto, M.; Villanueva, F.Y.; Cannizzo, A.; Naccache, R. Elucidating the mechanism of dual-fluorescence in carbon dots. *J. Colloid Interface Sci.* **2022**, *606*, 67–76. [CrossRef] [PubMed]
63. Wang, G.; Guo, G.L.; Chen, D.; Liu, Z.D.; Zheng, X.H.; Xu, A.L.; Yang, S.W.; Ding, G.Q. Facile and Highly Effective Synthesis of Controllable Lattice Sulfur-Doped Graphene Quantum Dots via Hydrothermal Treatment of Durian. *ACS Appl. Mater. Interfaces* **2018**, *10*, 5750–5759. [CrossRef]
64. Li, X.M.; Lau, S.P.; Tang, L.B.; Ji, R.B.; Yang, P.Z. Sulphur doping: A facile approach to tune the electronic structure and optical properties of graphene quantum dots. *Nanoscale* **2014**, *6*, 5323–5328. [CrossRef]
65. Yuan, Y.H.; Liu, Z.X.; Li, R.S.; Zou, H.Y.; Lin, M.; Liu, H.; Huang, C.Z. Synthesis of nitrogen-doping carbon dots with different photoluminescence properties by controlling the surface states. *Nanoscale* **2016**, *8*, 6770–6776. [CrossRef]